Journal of Molecular Liquids 218 (2016) 484–493

Contents lists available at ScienceDirect

Journal of Molecular Liquids

journal homepage: www.elsevier.com/locate/molliq

Simultaneous effects of nanoparticles and slip on Jeffrey fluid through tapered artery with mild stenosis

S.U. Rahman [a], R. Ellahi [b,c,*], S. Nadeem [d], Q.M. Zaigham Zia [e]

[a] Department of Mechatronics, UET Taxila, Chakwal Campus, Pakistan
[b] Department of Mathematics and Statistics, FBAS, IIUI, Islamabad, Pakistan
[c] Department of Mechanical Engineering, University of California Riverside, USA
[d] Department of Mathematics, Quaid-i-Azam University Islamabad, Pakistan
[e] Department of Mathematics, COMSATS Institute of Information Technology Chak Shazad Islamabad, Pakistan

ARTICLE INFO

Article history:
Received 23 January 2016
Accepted 24 February 2016
Available online xxxx

Keywords:
Nanoparticles
Jeffrey fluid
Convection
Slip
Blood flow
Tapered artery
Stenosed

ABSTRACT

This study examines the effects of nanoparticles for the blood flow of Jeffrey fluid in tapered artery with stenosis. The slip effects along with permeable nature of the arterial wall in the presence of convection are also taken into account. Mathematical modeling is based upon continuity, momentum and energy equations. This analysis is carried out under the constraints of mild stenosis. Closed form solutions for velocity and concentration are obtained. Numerical integration is used to analyze the novel features of flow impedance, pressure rise and stream function. Effects of pertinent parameters such as Brownian diffusion coefficient, thermospheric diffusion parameter, Grashof number and material constant of Jeffrey fluid on velocity, temperature and concentration are discussed through graphs.

1. Introduction

Blood is driven through the body by a complex network of veins and arteries. It is constantly in motion as the heart pumps blood through arteries to the different organs and cells of the body. It turns back to heart by veins. The veins are squeezed when muscles in the body contract and push the blood back to the heart. Stenosis is an abnormal narrowing in a blood vessel or other tabular organ or structure. It is also sometimes called a stricture. Most of the times these stenosis cause death when the degree of narrowing becomes significant enough to impede the flow of blood. Due to stenosis in the human artery, the flow of blood is disturbed and resistance to flow becomes higher than that of normal one. The main cause of formation of such stenosis is not yet known clearly but their consequences can be recognized easily.

Complete understanding of flow of blood through arteries of various geometries demands the basics concepts of mechanics of fluid. Some of the basic studies dealing different models of Newtonian and non-Newtonian fluids are given in references [1–6]. Several investigators have highlighted different aspects of blood flow analysis in arteries. Noreen [7] has examined the heat and mass transfer effects on Careau fluid model for blood flow through tapered arteries with stenosis. Mekheimer and El Kot [8] have studied the mathematical modeling of unsteady flow of fluid through anisotropically tapered elastic arteries with time variant overlapping stenosis. They analytically solved their mathematically model for mild stenosis case. Riahi et al. [9] have analyzed the problem of blood flow in an artery in the presence of an overlapping stenosis. A mathematical study on three layered oscillatory blood flow through stenosed arteries has been investigated by Tripathi [10]. Mishra et al. [11] have studied the blood flow through a composite stenosis in an artery with permeable wall.

It is well accepted now that slip effects may appear for two types of fluids (i.e., rare field gases [12] and fluids having much more elastic character). In these fluids, slippage appears as a result of large tangential traction. It is noticed through experiment observations [13–19] that the occurrence of slippage is possible in the non-Newtonian fluids (i.e. polymer solution and molten polymer). In addition, a clear layer is sometimes found next to the wall when flow of dilute suspension of particles is examined. In experimental physiology such a layer is observed when blood flow through capillary vessels is studied [20]. The fluids that exhibit slip effect have many applications, for instance, the polishing of artificial heart valves and internal cavities [21]. Moreover, the slip phenomenon is supported by the molecular theories [22–25].

In recent years, some interest has been promoted to the study of nanofluids. Nanotechnology has been widely used in industry since materials with sizes of nanometers possess unique physical and chemical properties. Nano-scale particle added fluids are called as nanofluid,

* Corresponding author at: Department of Mechanical Engineering, University of California Riverside, USA.
E-mail addresses: rellahi@engr.ucr.edu, rahmatellahi@yahoo.com (R. Ellahi).

http://dx.doi.org/10.1016/j.molliq.2016.02.080
0167-7322/

Nomenclature

u,v	velocity components
μ	viscosity
p	pressure
ρ	density
ξ	tapering parameter
δ	height of the stenosis
C_1	concentration
T_1	temperature
R_0	radius of non-tapered artery
d_0	radius of tapered artery
D_B	Brownian diffusion coefficient
D_T	thermospheric diffusion coefficient
N_t	thermophoresis parameter
N_b	Brownian motion parameter
G_r	Grashof number
L	finite length of tube
c	volumetric volume expansion coefficient
l	linear operator
q	embedding parameter

which is firstly introduced by Choi [26]. Choi et al. [27] showed that the addition of a small amount less than 1% by volume of nanoparticles to convectional heat transfer liquids increased the thermal conductivity of the fluid up to approximately two times. Khanafer et al. [28] seem to be the first who have examined heat transfer performance of nanofluids inside an enclosure taken into account the solid particle dispersion. After these studies, nanotechnology is considered by many to be one of the significant forces that drive the next major industrial revolution in the entire world. Currently, convective heat transfer in nanofluids is a topic of major contemporary interest in biological sciences. Some numerical and experimental studies on nanofluids include thermal conductivity are listed in [29–33].

In short, no such analysis is available in the literature which can describe the combined effects of slip, heat convection and nanoparticles for the flow of Jeffrey fluid in the tapered artery with stenosis. Motivated by these facts, the present work has been undertaken for the said purpose. To derive the solutions of nonlinear coupled equations, we have used one of the most effective methods, homotopy perturbation method (HPM). This method is not only valid for small (or large) values of physical parameter but also provides us a simple way to ensure the convergence of series solutions of a nonlinear problem. Some relevant studies on the topic can be seen from the list of references [34–37]. The paper is organized as follows. Section 2 contains the formulation of the problem. In Section 3 solution of the problem is obtained using HPM. Results and discussion are given in Section 4. This section devoted to analyzed, four cases namely, impedance variation, shear stress, variation in velocity distribution and variation in temperature and concentration distributions. The trapping phenomenon is also presented at the end. The conclusion is given in Section 5. Finally the physical features of the major parameters have been illustrated through graphs.

2. Formulation of the problem

Consider an incompressible nanofluid of viscosity μ and density ρ flowing through a tube having finite length L with overlapping stenosis. Let (r,θ,z) be the coordinates of a material point in the cylindrical polar coordinate system. Here $z-$ axis is taken along the axis of artery while r,θ are along the radial and circumferential direction respectively. Moreover $r=0$ is taken as the axis of symmetry of the tube. Heat and nanoparticle phenomenon are taken into account by giving temperature T_1 and concentration C_1 to the wall of the tube. At the centre of the tube, we consider symmetric conditions for velocity, temperature

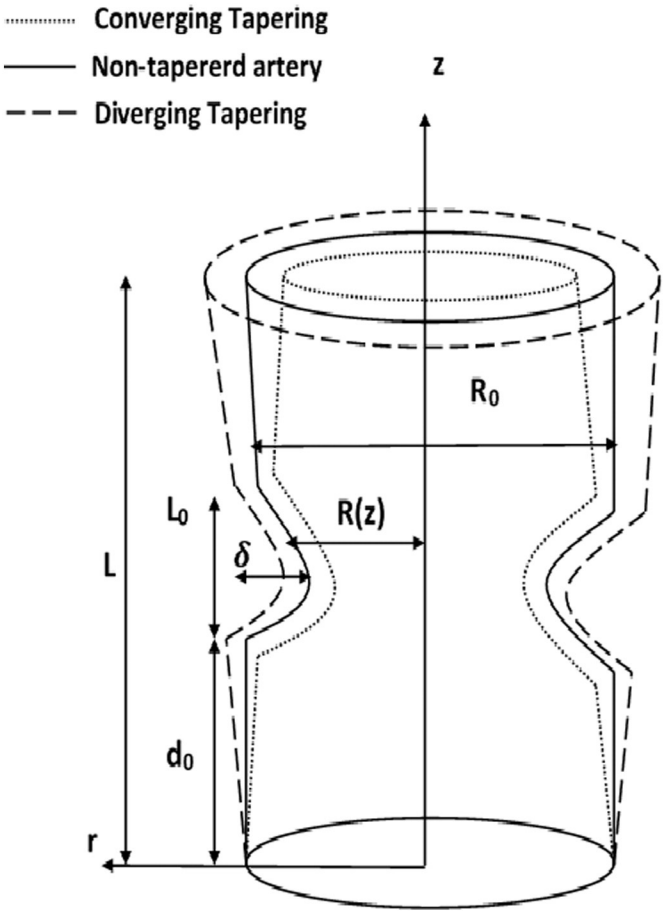

Fig. 1. Geometry of the stenosed tapered artery for different tapering angle.

and concentration. The geometry of the arterial wall of overlapping stenosis for different tapering angles [38,39] is defined as

$$R(z) = d(z)\left[1-\psi\left(L_0^{n-1}(z-d_0)-(z-d_0)^n\right)\right], d_0 < z \le d_0 + L_0, \\ = d(z), \text{otherwise} \tag{1}$$

with

$$\psi = \frac{\delta n^{\frac{n}{n-1}}}{R_0 L_0^n (n-1)}, \tag{2}$$

$$d(z) = R_0 + \xi z, \tag{3}$$

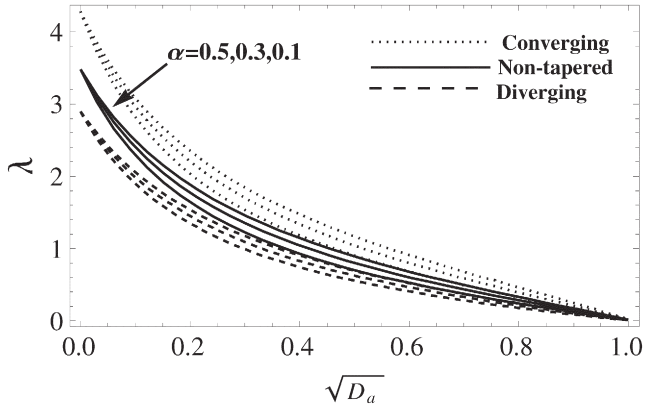

Fig. 2. Variation in impedance λ against $\sqrt{D_a}$ for $\alpha=0.1,0.3,0.5$.

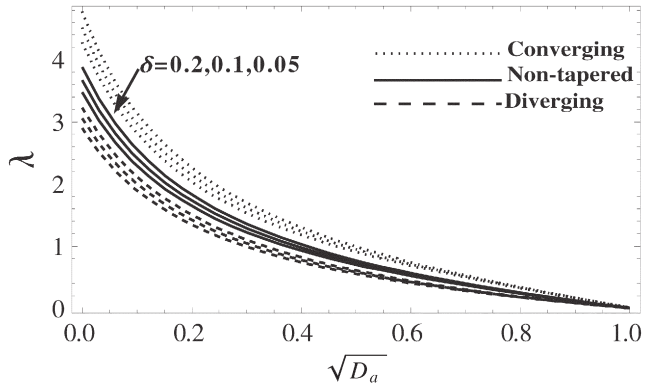

Fig. 3. Variation in impedance λ against $\sqrt{D_a}$ for $\delta = 0.05, 0.1, 0.2$.

in which δ denotes the maximum height of the stenosis located at

$$z = d_0 + \frac{L_0}{n^{\frac{n-1}{n}}}, \tag{4}$$

where R_0 is the radius of non-tapered artery in non-stenotic region. ξ is the tapering parameter and L_0 is the length of stenosis. The constant parameter $n(\geq 2)$ is responsible to determine the shape of constriction profile referred to as shape parameter for which symmetric stenosis is found for $n = 2$. The radius d_0 of tapered arterial segment in stenotic region indicates the location of stenosis as shown in Fig. 1.

The equations for unsteady flow of an incompressible nano fluid in the presence of body force are given by

$$\frac{1}{r}\frac{\partial(rv)}{\partial r} + \frac{\partial u}{\partial z} = 0, \tag{5}$$

$$\rho\left(v\frac{\partial v}{\partial r} + u\frac{\partial v}{\partial z}\right) = -\frac{\partial p}{\partial r} + \frac{1}{r}\frac{\partial}{\partial r}(rS_{rr}) + \frac{\partial}{\partial z}(S_{rz}) - \frac{1}{r}S_{\theta\theta}, \tag{6}$$

$$\rho\left(v\frac{\partial u}{\partial r} + u\frac{\partial u}{\partial z}\right) = -\frac{\partial p}{\partial z} + \frac{1}{r}\frac{\partial}{\partial r}(rS_{rz}) + \frac{\partial}{\partial z}(S_{zz}) + \rho g\alpha_1(T - T_1) + \rho g\alpha_1(C - C_1), \tag{7}$$

$$\left(v\frac{\partial T}{\partial r} + u\frac{\partial T}{\partial z}\right) = \alpha_1\left(\frac{\partial^2 T}{\partial r^2} + \frac{1}{r}\frac{\partial T}{\partial r} + \frac{\partial^2 T}{\partial z^2}\right) + \tau\left[\begin{array}{l} D_B\left(\frac{\partial C}{\partial r}\frac{\partial T}{\partial r} + \frac{\partial C}{\partial z}\frac{\partial T}{\partial z}\right) \\ +\frac{D_T}{T_0}\left(\left(\frac{\partial T}{\partial r}\right)^2 + \left(\frac{\partial T}{\partial z}\right)^2\right) \end{array}\right], \tag{8}$$

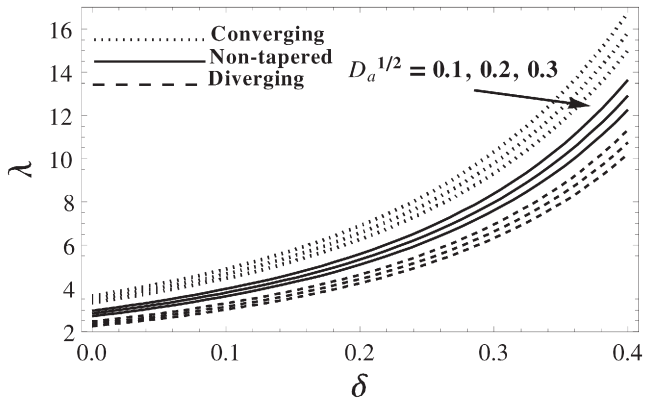

Fig. 4. Variation in impedance λ against δ for $\sqrt{D_a} = 0.1, 0.2, 0.3$.

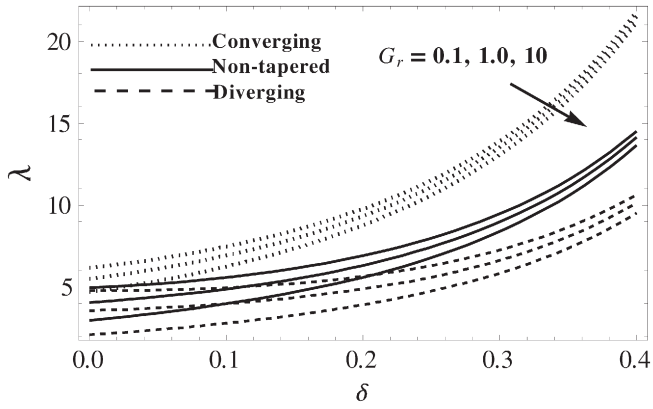

Fig. 5. Variation in impedance λ against δ for $G_r = 0.1, 1.0, 10$.

$$\left(v\frac{\partial C}{\partial r} + u\frac{\partial C}{\partial z}\right) = D_B\left(\frac{\partial^2 C}{\partial r^2} + \frac{1}{r}\frac{\partial C}{\partial r} + \frac{\partial^2 C}{\partial z^2}\right) + \frac{D_T}{T_0}\left(\frac{\partial^2 T}{\partial r^2} + \frac{1}{r}\frac{\partial T}{\partial r} + \frac{\partial^2 T}{\partial z^2}\right). \tag{9}$$

Here $\tau = (\rho c)_p/(\rho c)_f$ is the ratio between effective heat capacity of nano particle material and heat capacity of the fluid, c is the volumetric volume expansion coefficient, u and v are the axial and radial velocities respectively, p is the pressure C is the nanoparticle phenomena. D_B is the Brownian diffusion coefficient, D_T is the thermospheric diffusion coefficient, the ambient values of T and C as r tends to R are denoted by T_1 and C_1 respectively.

$$S_{rr} = \frac{2\mu}{1+\lambda_1}\left(1 + \lambda_2\left(v\frac{\partial}{\partial r} + u\frac{\partial}{\partial z}\right)\right)\frac{\partial v}{\partial r}, \tag{10}$$

$$S_{rz} = \frac{\mu}{1+\lambda_1}\left(1 + \lambda_2\left(v\frac{\partial}{\partial r} + u\frac{\partial}{\partial z}\right)\right)\left(\frac{\partial v}{\partial z} + \frac{\partial u}{\partial r}\right), \tag{11}$$

$$S_{zz} = \frac{2\mu}{1+\lambda_1}\left(1 + \lambda_2\left(v\frac{\partial}{\partial r} + u\frac{\partial}{\partial z}\right)\right)\frac{\partial u}{\partial z}. \tag{12}$$

Introducing the following non-dimensional variables

$$\left.\begin{array}{l} \overline{r} = \frac{r}{R_0}, \overline{z} = \frac{z}{L_0}, \overline{v} = \frac{L_0}{\delta U}v, u = \frac{u}{U}, \overline{R} = \frac{R}{R_0}, \overline{p} = \frac{R_0^2}{UL_0\mu}p, \\ T = T_1 + (T_0 - T_1)\theta, C = C_1 + (C_0 - C_1)\sigma, G_r = \frac{\rho g\alpha_1 R_0^3 T_1}{\mu}, \\ B_r = \frac{\rho g\alpha_1 R_0^3 T_1}{\mu},\ N_t = \frac{(\rho c)_p D_T T_0}{(\rho c)_f \alpha_1}, N_b = \frac{(\rho c)_p D_T C_0}{(\rho c)_f \alpha_1}, R_e = \frac{\rho U R_0}{\mu} \end{array}\right\} \tag{13}$$

in which U is the velocity over the section of tube with radius R_0. N_t, N_b, G_r and B_r are respectively the thermophoresis parameter, the Brownian

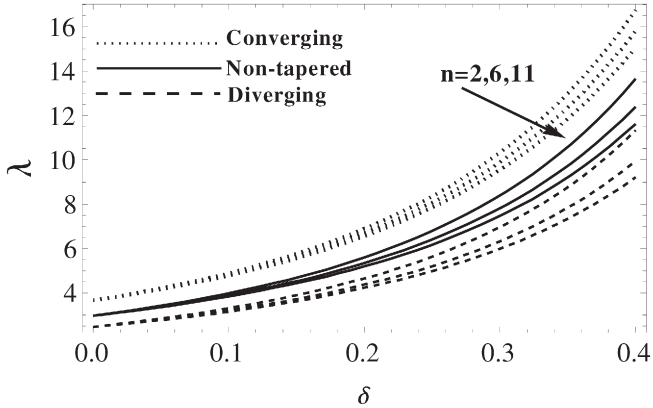

Fig. 6. Variation in impedance λ against δ for $n = 2, 6, 11$.

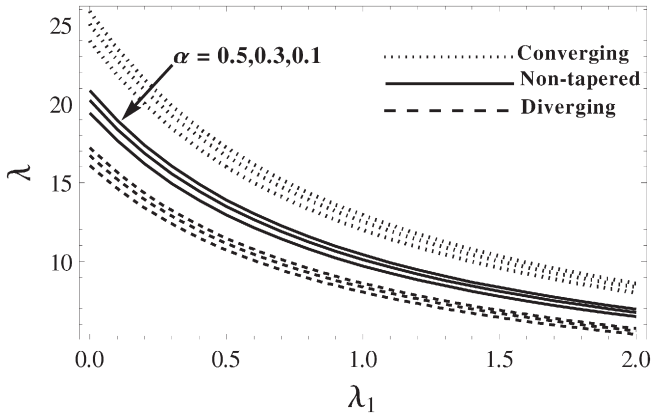

Fig. 7. Variation in impedance λ against λ_1 for $\alpha = 0.1, 0.3, 0.5$.

motion parameter, the local temperature Grashof number and the local nanoparticle Grashof number. Making use of these variables in Eqs. (5) to (9) and after applying the additional condition $\varepsilon = R_0/L_0 = o(1)$ for the case of mild stenosis ($\delta^* = \delta/R_0 << 1$), the non-dimensional governing equations after dropping the dashes can be written as

$$\left(\frac{\partial v}{\partial r} + \frac{v}{r}\right)\delta^* + \frac{\partial u}{\partial z} = 0, \tag{14}$$

$$\frac{\partial p}{\partial r} = 0, \tag{15}$$

$$\frac{\partial p}{\partial z} = \frac{1}{r}\frac{\partial}{\partial r}\left(\frac{r}{1+\lambda_1}\left(\frac{\partial u}{\partial r}\right)\right) + G_r\theta + B_r\sigma, \tag{16}$$

$$\frac{1}{r}\frac{\partial}{\partial r}\left(r\frac{\partial \theta}{\partial r}\right) + N_b\frac{\partial \sigma}{\partial r}\frac{\partial \theta}{\partial r} + N_t\left(\frac{\partial \theta}{\partial r}\right)^2 = 0, \tag{17}$$

$$N_b\frac{\partial}{\partial r}\left(r\frac{\partial \sigma}{\partial r}\right) + N_t\frac{\partial}{\partial r}\left(r\frac{\partial \theta}{\partial r}\right) = 0. \tag{18}$$

The non-dimensional boundary conditions on velocity for permeable wall are

$$\frac{\partial u}{\partial r} = 0 \text{ at } r = 0, \tag{19}$$

$$u = u_B, \frac{\partial u}{\partial r} = \frac{\alpha}{\sqrt{D_a}}(u_B - u_p) \text{ at } r = R(z), \tag{20}$$

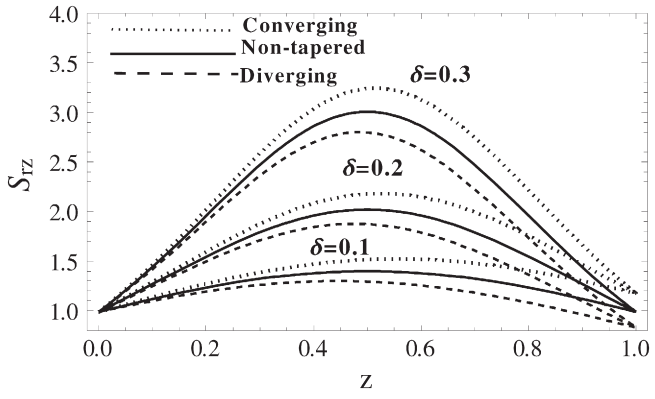

Fig. 8. Variation in stress S_{rz} against radius z for $\delta = 0.1, 0.2, 0.3$.

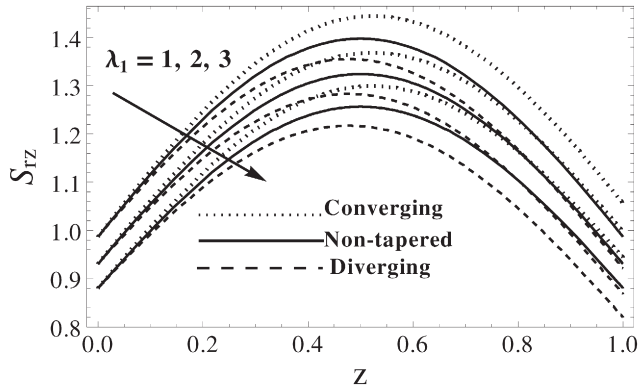

Fig. 9. Variation in stress S_{rz} against radius z for $\lambda_1 = 1, 2, 3$.

where u_B is the slip velocity to be determined. The non-dimensional conditions for θ and σ are

$$\frac{\partial \theta}{\partial r} = 0, \frac{\partial \sigma}{\partial r} = 0, \text{ at } r = 0, \tag{21}$$

$$\theta = 0, \sigma = 0 \text{ at } r = R(z). \tag{22}$$

Eq. (1) reduces to

$$R(z) = (1+\xi_1 z)\left[1 - \psi_1\left((z-d_0^*) - (z-d_0^*)^n\right)\right], d_0^* < z \le d_0^* + 1, \\ = (1+\xi_1 z), \text{otherwise} \tag{23}$$

where

$$d_0^* = \frac{d_0}{L_0}, \xi_1 = \frac{\xi L_0}{R_0}, \psi_1 = \frac{\delta^* n^{\frac{n}{n-1}}}{(n-1)}. \tag{24}$$

3. Solution of the problem

Our interest in this section is to carry out analytical solutions of the coupled Eqs. (17) and (18) using homotopy perturbation method. For series solutions up to second order, we expand θ and σ in terms of embedding parameter q as follows:

$$\theta(r,z) = \theta_0 + q\theta_1 + q^2\theta_2 + \ldots \tag{25}$$

$$\sigma(r,z) = \sigma_0 + q\sigma_1 + q^2\sigma_2 + \ldots. \tag{26}$$

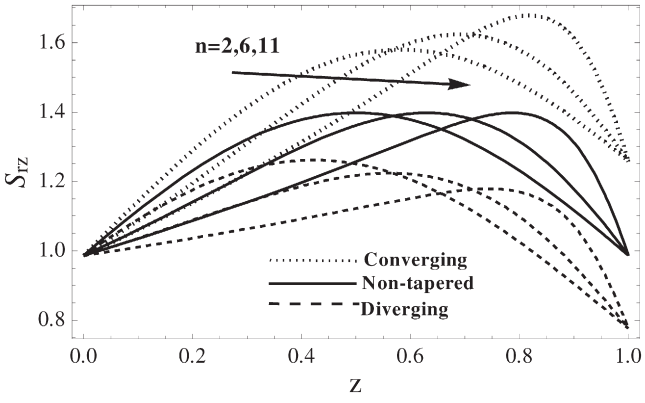

Fig. 10. Variation in stress S_{rz} against radius z for $n = 2, 6, 11$.

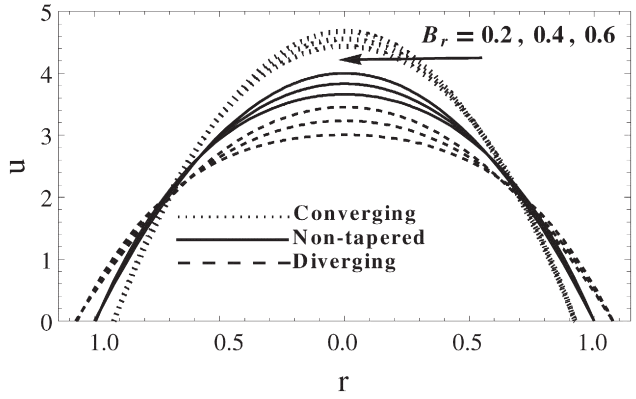

Fig. 11. Variation in velocity u against radius r for $B_b = 0.2, 0.4, 0.6$.

Let us construct the homotopy

$$H(q,\theta) = (1-q)\,[l(\theta) - l(\theta_0)] + q\left[l(\theta) + N_b\frac{\partial\sigma}{\partial r}\frac{\partial\theta}{\partial r} + N_t\left(\frac{\partial\theta}{\partial r}\right)^2\right], \tag{27}$$

$$H(q,\theta) = l(\theta) - l(\theta_0) + ql(\theta) + q\left[N_b\frac{\partial\sigma}{\partial r}\frac{\partial\theta}{\partial r} + N_t\left(\frac{\partial\theta}{\partial r}\right)^2\right], \tag{28}$$

$$H(q,\sigma) = (1-q)\,[l(\sigma) - l(\sigma_0)] + q\left[l(\sigma) + \frac{N_t}{N_b}\left(\frac{1}{r}\frac{\partial}{\partial r}\left(r\frac{\partial\theta}{\partial r}\right)\right)\right], \tag{29}$$

$$H(q,\sigma) = l(\sigma) - l(\sigma_0) + ql(\sigma_0) + q\left[\frac{N_t}{N_b}\left(\frac{1}{r}\frac{\partial}{\partial r}\left(r\frac{\partial\theta}{\partial r}\right)\right)\right], \tag{30}$$

where $q \in [0,1]$. For HPM solution we select

$$\theta_0(r,z) = \left(\frac{r^2-R^2}{4}\right), \sigma_0(r,z) = -\left(\frac{r^2-R^2}{4}\right) \tag{31}$$

as the initial approximation of θ and σ respectively which satisfy the following linear operator and corresponding boundary conditions. The solutions for temperature and concentration for $q = 1$, can thus obtained as

$$\theta(r,z) = \frac{1}{64}(N_b - N_t)\left(r^2-R^2\right) - \left[\begin{array}{l}\frac{1}{18}N_b\left(r^3-R^3\right)\\ +\frac{N_t}{36864}\left(N_b^2+N_t^2\right)\left(r^4-R^4\right)\left(r^6-R^6\right)\end{array}\right], \tag{32}$$

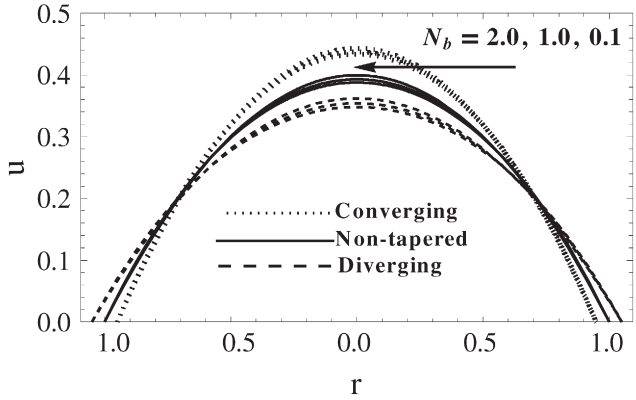

Fig. 12. Variation in velocity u against radius r for $N_b = 2.0, 1.0, 0.1$.

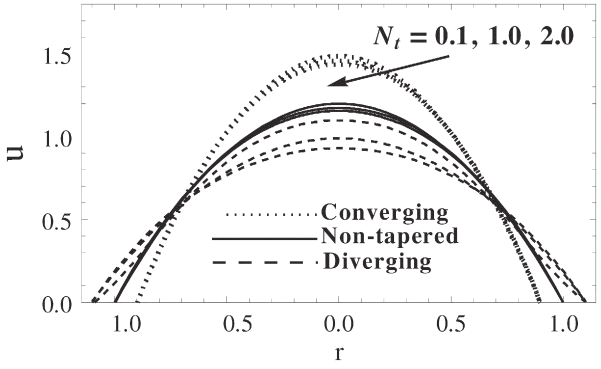

Fig. 13. Variation in velocity u against radius r for $N_t = 1, 2, 3$.

$$\sigma(r,z) = -\frac{1}{4}\left(r^2-R^2\right)\frac{N_t}{N_b} + \frac{N_t}{N_b}\left(\frac{1}{18}N_b\left(r^3-R^3\right) + \frac{1}{36864}\left(N_b^2+N_t^2\right)\left(r^6-R^6\right)\right). \tag{33}$$

Substituting Eqs. (32) and (33) in Eq. (16), the exact solution for velocity is obtained as

$$u(r,z) = \left\{\begin{array}{l}\frac{1}{530841600nb}(-25bN_t\left(r^2-R^2\right)(4r^2\left(82944+N_t^3r^8\right)\\ +4R^2\left(-248832+N_t^3r^8\right)-5N_t^3r^6R^4-21N_t^3r^4R^6\\ -21N_t^3r^2R^8+123N_t^3R^{10}\right)(1+\lambda_1)-25G_rN_b^3N_t\\ \left(4r^{12}-9r^8R^4-16r^6R^6+144r^2R^{10}-123R^{12}\right)\\ (1+\lambda_1)+25N_b^2\left(r^2-R^2\right)\\ \left(B_rN_t^2(4r^{10}+4r^8R^2-5r^6R^4-21r^4R^6-21r^2R^8+123R^{10}\right)\\ +9216G_r(r^4+r^2\left(R^2-8\right)-8R^2\left(R^2-3\right)))\\ (1+\lambda_1)+N_b(530841600u_B+132710400\\ \frac{dp}{dz}\left(r^2-R^2\right)(1+\lambda_1)+N(_t294912B_r\\ \left(4r^5-25r^2R^2+21R^5\right)+25G_r\left(4N_t^2r^{12}-9N_t^2r^8R^4-16r^6\right.\\ \left(576+N_t^2R^6\right)+144r^2R^4\left(576+N_t^2R^6\right)\\ \left.-3R^6\left(24576+41N_t^2R^6\right)\right)(1+\lambda_1)),\end{array}\right\}, \tag{34}$$

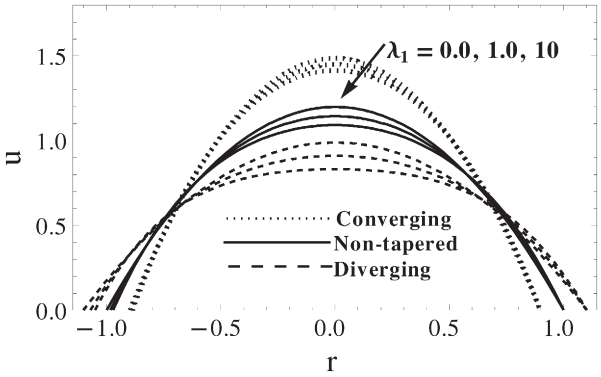

Fig. 14. Variation in velocity u against radius r for $\lambda_1 = 0.0, 1.0, 10$.

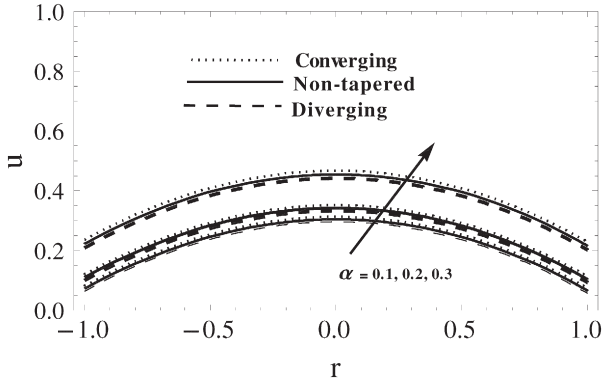

Fig. 15. Variation in velocity u against radius r for $\alpha = 0.1, 0.2, 0.3$.

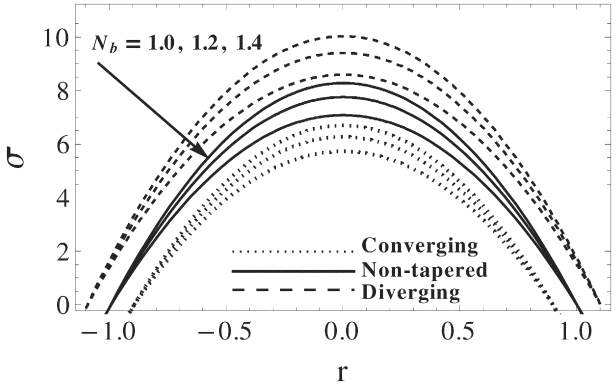

Fig. 17. Variation in concentration σ against radius r for $N_b = 1.0, 1.2, 1.4$.

where

$$u_B = \frac{1}{4423680N_b\alpha} \times \left(4423680N_b\alpha u_p - \sqrt{D_a}R\left(-2211840N_b\frac{dp}{dz} - 30720\left(2G_rN_b^2 + 9B_rN_t\right)\right)R^2 + \begin{matrix} 73728B_rN_tN_bR^3 + 23040G_rN_b(N_b - N_t)R^4 \\ +35N_t(B_rN_t - G_rN_b)\left(N_t^2 - N_b^2\right)R^{10} \end{matrix}\right)(1+\lambda_1)\Bigg), \tag{35}$$

$$u_p = -\frac{D_a}{\mu}\frac{dp}{dz}. \tag{36}$$

The flux Q can be calculated as

$$Q = 2\int_0^R rudr, \tag{37}$$

$$Q = \left(-\frac{\partial p}{\partial z}\right)\frac{1}{F(z)}. \tag{38}$$

Impedance λ is calculated as

$$\lambda = \frac{1}{Q}\int_0^7 \left(-\frac{\partial p}{\partial z}\right)dz, \tag{39}$$

$$\overline{\lambda} = \int_0^{d0}\frac{1}{F(z)}dz + \int_{d0}^{d_0+L_0}\frac{1}{F(z)}dz + \int_{d_0+L_0}^{L}\frac{1}{F(z)}dz, \tag{40}$$

$$\overline{\lambda} = (L - L_0)\frac{1}{F(z)/_{R=1}} + \int_{d_0}^{d_0+L_0}\frac{1}{F(z)}dz, \tag{41}$$

$$\frac{\overline{\lambda}}{L} = \left(1 - \frac{L_0}{L}\right)\frac{1}{F(z)/_{R=1}} + \frac{1}{L}\int_{d_0}^{d_0+L_0}\frac{1}{F(z)}dz, \tag{42}$$

The impedance per unit length of the artery

$$\lambda = \left(1 - \frac{L_0}{L}\right)\frac{1}{F(z)/_{R=1}} + \frac{1}{L}\int_{d_0}^{d_0+L_0}\frac{1}{F(z)}dz. \tag{43}$$

The nonzero dimensionless shear stress in our problem is given by

$$S_{zr} = -\frac{R}{2}\frac{\partial p}{\partial z}, \tag{44}$$

The expression for wall shear stress can be calculated as

$$S_{rz} = -\frac{R}{2}\left(\frac{\partial p}{\partial z}\right)_{r=R}. \tag{45}$$

4. Results and discussion

This section describes the graphical features of pertinent parameters on the profiles of impedance (λ), shear stress (S_{rz}), velocity (u), concentration (σ) and temperature (θ). The observations are made for converging tapering, non-tapered artery and diverging tapering to see the effects under different shapes of stenosis. The graphs of impedance

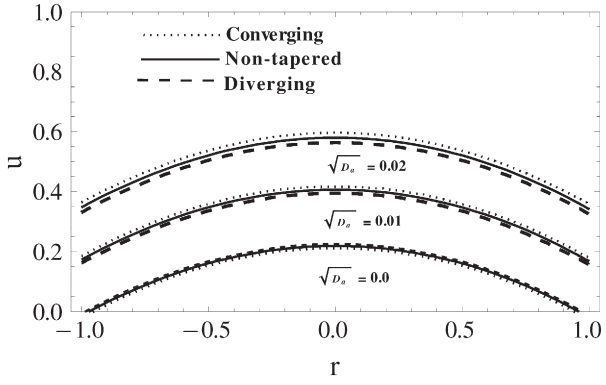

Fig. 16. Variation in velocity u against radius r for $\sqrt{D_a} = 0.00, 0.01, 0.02$.

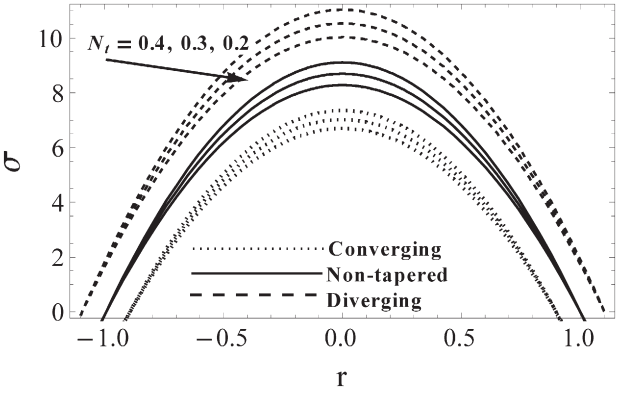

Fig. 18. Variation in concentration σ against radius r for $N_t = 0.4, 0.3, 0.2$.

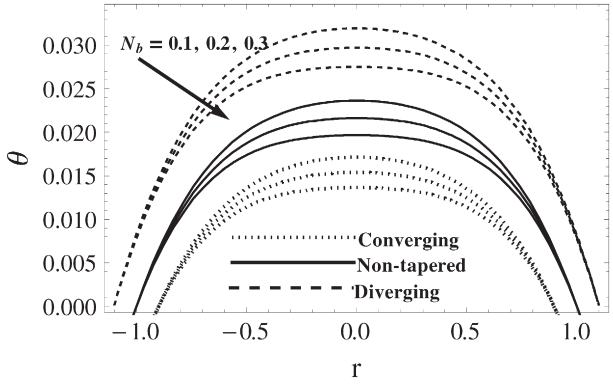

Fig. 19. Variation in temperature θ against radius r for $N_b = 0.1, 0.2, 0.3$.

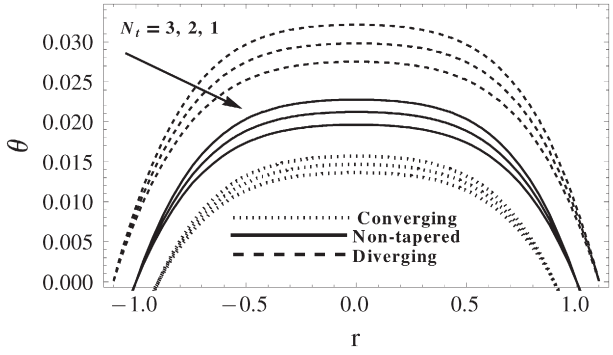

Fig. 20. Variation in temperature θ against radius r for $N_t = 3, 2, 1$.

(λ) are drawn against the Darcy number ($\sqrt{D_a}$), Jeffrey fluid parameter (λ_1) and stenosis height (δ) for different values of (α), (δ), ($\sqrt{D_a}$), (G_r) and (n). Wall shear stress S_{rz} is plotted against axial coordinate z and influences of (δ), (λ_1) and (n) are characterized. The velocity profile u is examined against radial coordinate r and effects of (B_r), (N_b), (λ_1), (α), ($\sqrt{D_a}$) and (N_t) are discussed. Variation in concentration (σ) is discussed for various values of (N_b) and (N_t). Influence on temperature profile (θ) also examined for different values (N_b) and (N_t). The streamlines are displayed in the end to investigate the flow pattern under the presence of different parameters to discuss the trapping bolus phenomenon.

4.1. The impedance profile

In Fig. 2, the impedance is plotted for the variation of the slip parameter α against the Darcy number $\sqrt{D_a}$. It is revealed here that impedance of the flow is larger in the domain $0<\sqrt{D_a}<0.4$ as compared with the rest of the regions. It is also seen that impedance has indirect relation with the variation of slip parameter for three different types of arterial shapes. The altitude of the impedance profile is getting higher for diverging tapering, non-tapered artery and converging tapering, respectively. One can see the impact of δ on the distribution of impedance against the Darcy number in Fig. 3. From this graph, it is measured that impedance is increasing with the increase in δ but no much variation in the impedance is observed in the region $0.8<\sqrt{D_a}<1.0$.Fig. 4 implies the influence of $\sqrt{D_a}$ on the impedance plotted along the stenosis height δ. It is concluded here that impedance is very small in the region $0<\delta<0.1$ and a significant variation is observed in the remaining part of the domain. It is noticed that $\sqrt{D_a}$ plays an inverse role in the variation of impedance for diverging tapering, non-tapered artery and converging tapering accordingly. Effects of G_r on impedance λ are seen in Fig. 5. The converging lines for different values of G_r assure that in the region $\delta>0.4$, they surely intersect and impedance λ will attain a fixed value there. In the domain $\delta<0.4$, increasing values of G_r decay the impedance. Influences of stenosis shape n and slip parameter α on impedance λ are examined in Figs. 6 and 7. Slip parameter enhances the impedance and a peak value of impedance is seen for the symmetric stenosis ($n=2$).

4.2. The shear stress profile

In Fig. 8 the effects of different stenosis height (δ) on the shear stress distribution is analyzed. It is depicted from this graph that stress is directly proportional to the stenosis height i.e., if we increase the stenosis height, the stress will get the higher amplitude. Fig. 9 corresponds to the variation of shear stress S_{rz} against the axial direction z under the effects of λ_1. Larger value of λ_1 causes in less impedance. Effects of stenosis shape parameter n is examined in Fig. 10. It is measured that in the region $0<z<0.6$, the stress decreases with n while in the other part, the inverse behavior is described by the stress profile for large values of n.

4.3. The velocity profile

The variation of axial velocity profile u for B_r is described in Fig. 11 which indicates that increasing values B_r decrease the velocity profile. The velocity profile u for N_b is presented in Fig. 12 plotted against the radial axis r. It suggests that velocity profile is rising with the increase in N_b but opposite attitude is reported for N_t (see Fig. 13). The larger values of Jeffrey parameter λ_1 decelerate the flow as shown in Fig. 14. The effects of slip parameter α and Darcy number $\sqrt{D_a}$ are displayed in Figs. 15 and 16.

4.4. The concentration and temperature profiles

Effects of N_b and N_t on concentration σ and temperature θ profiles are shown in Figs. 17 to 20 respectively. It is observed that by increasing

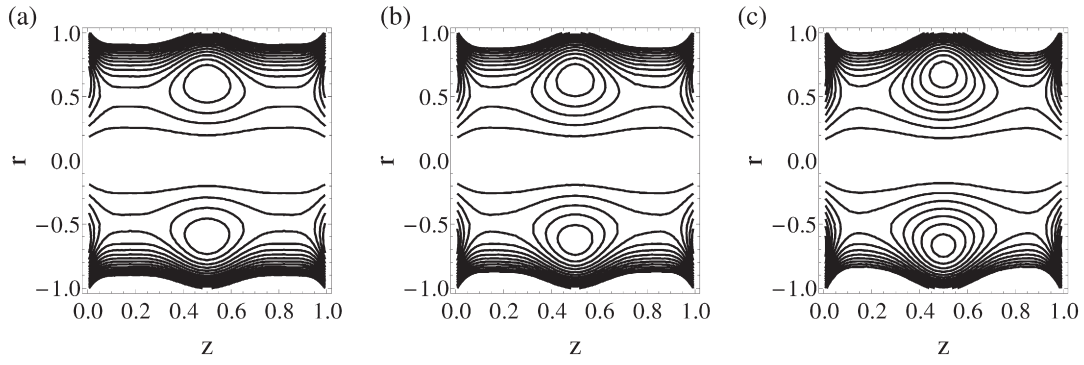

Fig. 21. Streamlines for α. (*a*) $\alpha=0.1$, (*b*) $\alpha=0.3$, (*a*) $\alpha=0.5$.

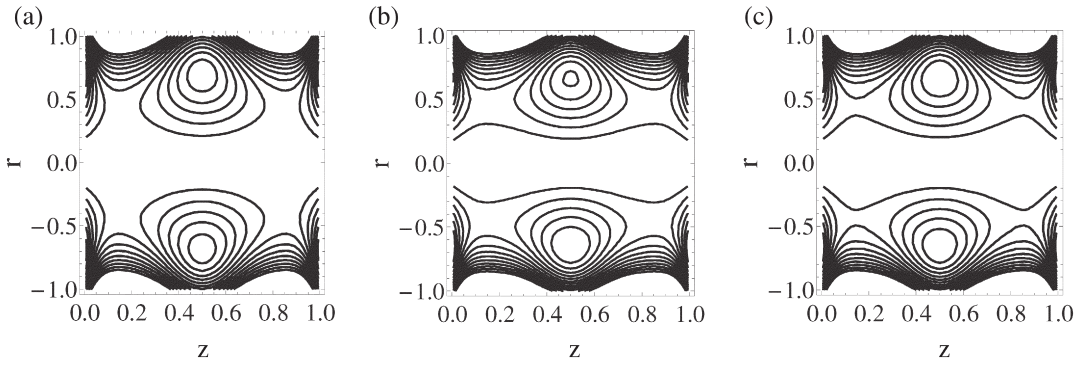

Fig. 22. Streamlines for $\sqrt{D_a}$. (*a*) $\sqrt{D_a} = 0.4$, (*b*) $\sqrt{D_a} = 0.5$, (*a*) $\sqrt{D_a} = 0.6$.

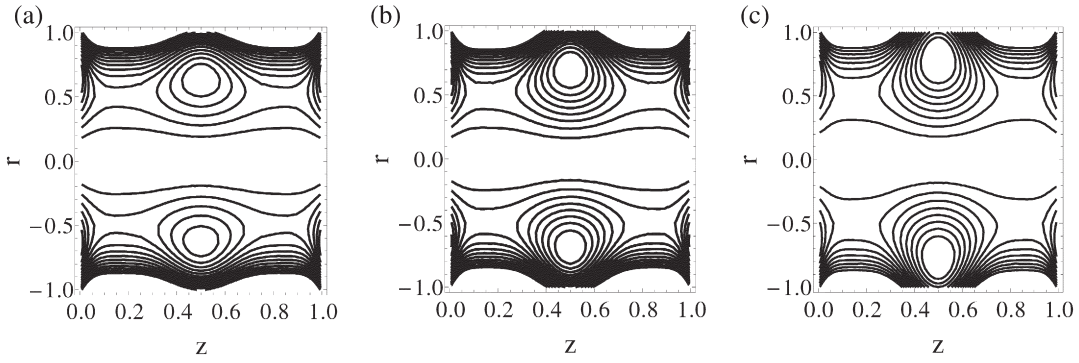

Fig. 23. Streamlines for δ. (*a*) $\delta = 0.10$, (*b*) $\delta = 0.20$, (*a*) $\delta = 0.30$.

N_b and decreasing N_t, concentration profile decreases. An increment in θ is observed by decreasing N_b and N_t.

4.5. Trapping phenomena

Fig. 21 shows the streamlines for the slip parameter α. It is seen here that as we increase the slip parameter, the area of the bolus is expanding and number of bolus is increased. The variation of Darcy number $\sqrt{D_a}$ for the streamlines is displayed in Fig. 22. It is noted that less boluses are obtained with the increase in magnitude of Darcy number but size of the bolus is increased gradually. Figs. 23 to 24 reveal the same behavior for δ and inverse behavior of streamlines with the variation of λ_1 as observed in the previous figure for Darcy number. It is resulted from Fig. 25 that boluses are decreased in size and their position is shifted from mean position as we disturb stenosis shape from symmetric to a non-symmetric by assigning $n = 2, 6, 11$ respectively. Furthermore, Fig. 26 is presented for best interest of readers. One can easily observe that how the stenosis shape vicissitudes for varying values of n which is in accordance with the physical expectation available in the existing literature.

5. Conclusion

The present study reveals the effects of heat and mass transfer on the blood flow of Jeffrey fluid through tapered artery with stenosis. The walls of the artery are taken permeable. The main observations of the performed analysis are as follows:

- The maximum impedance λ is offered by the symmetric stenosis $n = 2$.
- Slip parameter enhances the impedance for the symmetric stenosis.
- The slip parameter α and the Darcy number $\sqrt{D_a}$ have mutually opposite effects on impedance.
- Impedance of the flow is larger in the domain $0 < \sqrt{D_a} < 0.4$ as compared with the rest of regions.

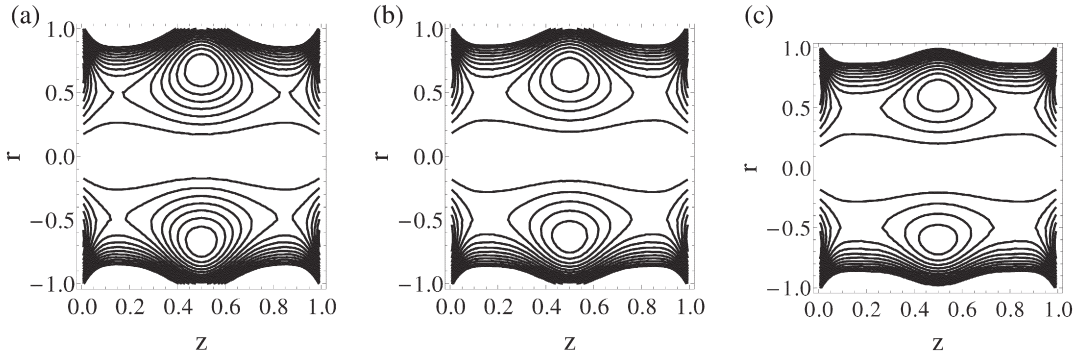

Fig. 24. Streamlines for λ_1. (*a*) $\lambda_1 = 0.10$, (*b*) $\lambda_1 = 0.5$, (*a*) $\lambda_1 = 0.9$.

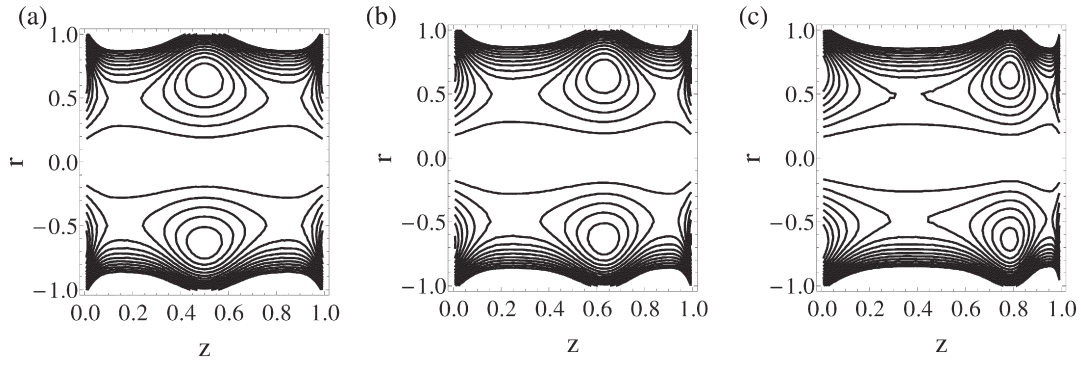

Fig. 25. Streamlines for *n*. (*a*) $n=02$, (*b*) $n=06$, (*a*) $n=11$.

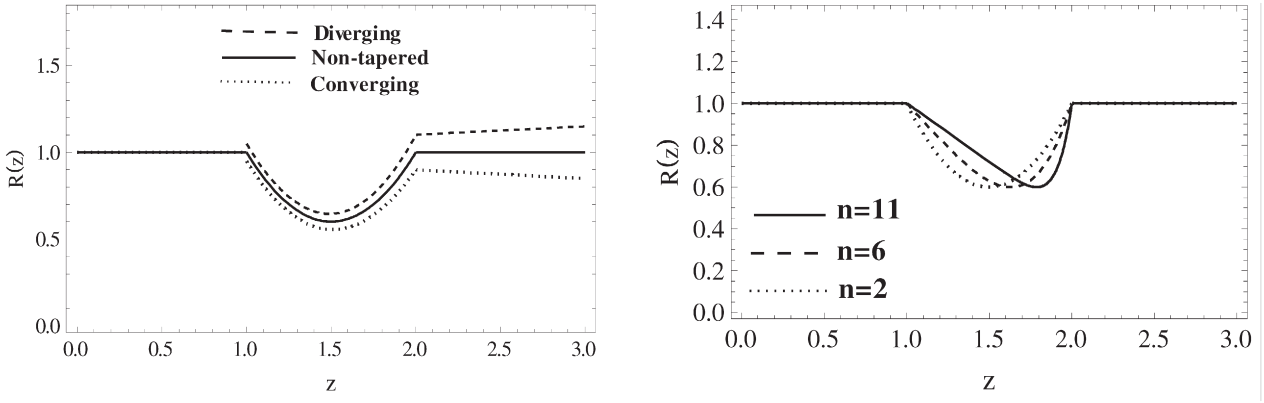

Fig. 26. Visual representation of stenosis.

- The altitude of the impedance profile is getting higher for diverging tapering, non-tapered artery and converging tapering, respectively.
- Grashof number G_r and mild stenosis δ have the same effects on impedance.
- Larger value of λ_1 causes in less impedance.
- Larger the stenosis height, greater the wall shear stress S_{rz} is observed.
- Increasing values of B_r decrease the velocity profile. It is seen that velocity profile is rising with the increase in N_b but opposite attitude is reported for N_t.
- The larger values of Jeffrey parameter λ_1 decelerate the velocity profile.
- The velocity exhibits same variation by varying B_r and N_b whereas the velocity, temperature and nano-concentrations decrease by increasing the thermophoresis parameter when Brownian diffusion coefficient is fixed and behave in an opposite manner is observed when one vary Brownian diffusion coefficient keeping thermophoresis parameter fixed. This is in accordance with the fact that for thermal boundary the effects of thermophoresis parameter and Brownian diffusion coefficient are different.
- The area of the bolus is expanding and number of bolus is increased for slip parameter whereas less boluses are obtained with the increase in magnitude of Darcy number but size of the bolus is increased gradually. Same behavior for δ and inverse behavior of streamlines with the variation of λ_1 is observed for Darcy number. It is noticed that the boluses are decreased in size and their position is shifted from mean position for different shape of stenosis.
- The obtained results for the flow of heat transfer characteristics expose many interesting behaviors that warrant further study on the non-Newtonian fluid phenomena, particularly the shear-thinning and shear-thickening phenomena.

References

[1] C. Fetecau, C. Fetecau, On some axial Couette flows of non-Newtonian fluids, Z. Angew. Math. Phys. 56 (2005) 1098–1106.
[2] Noreen Sher Akbar, Eyring Prandtl fluid flow with convective boundary conditions in small intestines, Int. J. Biomath. 6 (2013) 350034.
[3] I.A. Abbas, M.F. El-Amin, A. Salama, Effect of thermal dispersion on free convection in a fluid saturated porous medium, Int. J. Heat Fluid Flow 30 (2) (2009) 229–236.
[4] I.A. Abbas, M.F. El-Amin, A. Salama, Combined effect of thermal dispersion and radiation on free convection in a fluid saturated, optically thick porous medium, Forsch. Ingenieurwes. 72 (2008) 135–144.
[5] K. Rajneesh, I.A. Abbas, V. Sharma, A numerical study of free convection heat and mass transfer in a Rivlin–Ericksen viscoelastic flow past an impulsively started vertical plate with variable temperature and concentration, Int. J. Heat Fluid Flow 44 (2013) 258–264.
[6] I.A. Abbas, M.F. El-Amin, Shuyu Sun, Comparison study between the effects of different terms contributing to viscous dissipation in saturated porous media, Int. J. Therm. Sci. 64 (2013) 195–203.
[7] Noreen Sher Akbar, Heat and mass transfer effects on Careau fluid model for blood flow through tapered arteries with stenosis, Int. J. Biomath. 7 (2014) 1450004.
[8] Kh. Mekheimer, M.A. El kot, Mathematical modelling of unsteady flow of a Sisko fluid through an anisotropically tapered elastic arteries with time-variant overlapping stenosis, J. Appl. Math. Model. 36 (11) (2012) 5393–5407.
[9] D.N. Riahi, R. Roy, S. Cavazos, On arterial blood flow in the presence of an overlapping stenosis, Math. Comput. Model. 54 (11) (2011) 2999–3006.
[10] D.A. Tripathy, A mathematical study on three layered oscillatory blood flow through stenosed arteries, J. Bionic Eng. 9 (1) (2012) 119–131.
[11] S. Mishra, S.U.A. Siddiqui, A. Medhavi, Blood flow through a composite stenosis in an artery with permeable wall, Appl. Appl. Math. 6 (11) (2011) 58–73.
[12] W. Chu Kwang-Hua, J. Fang, Peristaltic transport in a slip flow, Eur. Phys. J. B 16 (2000) 543–547.
[13] G.V. Vinogradov, L.I. Ivanova, Wall slippage and elastic turbulence of polymers in the rubbery state, Rheol. Acta 7 (1968) 243–254.
[14] S. Luk, R. Mutharasan, D. Apelian, Experimental observations of wall slip: tube and packed bed flow, Ind. Eng. Chem. Res. 26 (1987) 1609–1616.
[15] N.E.L. Kissi, J.M. Piau, Ecoulement de fluides polymeres enchevetres dans un capillaire. Modelisation du glissement macroscopique a la paroi, C. R. Acad. Sci. Paris Ser II Mec. Phys. Chim. Sci. Univers Sci. Terre 309 (1989) 7–9.

[16] J.L. White, M.H. Han, N. Nakajima, R. Brazoskowski, The influence of materials of construction on biconical rotor and considerations of slippage, J. Rheol. 35 (1991) 167–189.
[17] S.G. Hatzikiriakos, J.M. Dealy, Wall slip of molten high density polyethylene II. Capillary rheometer studies, J. Rheology 36 (1992) 703–741.
[18] K.B. Migler, H. Hervet, L. Leger, Slip transition of a polymer melt under shear stress, Phys. Rev. Lett. 70 (1993) 287–290.
[19] J.M. Piau, N. EL, Kissi, measurement and modeling of friction in polymer melts during macroscopic slip at the wall, J. Non-Newtonian Fluid Mech. 54 (1994) 121–142.
[20] D.B. Coleman, H. Markovitz, W. Noll, Viscometer Flows of Non-Newtonian Fluid, Spring Verlag, Berlin, Heidelberg, New York, 1996.
[21] C. LE, Roux, existence and uniqueness of the flow of second grade fluids with slip boundary conditions, Arch. Ration. Mech. Anal. 148 (1999) 309–356.
[22] I. Leonov, On the dependence of friction force on sliding velocity in the theory of adhesive friction of elastomers, Wear 141 (1990) 137–145.
[23] M.A. Valdez, J. Tejero, Hydrodynamic interactions of dilute polymer solutions under shear flow in a narrow channel, Rheol. Acta 33 (1994) 125–135.
[24] S.G. Hatzikiriakos, A multimode interfacial constitutive equation for molten polymers, J. Rheol. 39 (1995) 61–71.
[25] R.L. Schiek, G.S.E. Shaqfeh, A nonlocal theory for stress in bound, Brownian suspensions of slender, rigid fibres, J. Fluid Mech. 296 (1995) 271–324.
[26] S.U.S. Choi, Enhancing thermal conductivity of fluids with nanoparticles, The Proceedings of the a995 ASME International Mechanical Engineering Congress and Exposition, 66, ASME, FED 231/MD, San Francisco, USA, 1995, pp. 99–105.
[27] S.U.S. Choi, Z.G. Zhang, W. Yu, F.E. Lockwood, E.A. Grulke, Anomalously thermal conductivity enhancement in nanotube suspensions, Appl. Phys. Lett. 79 (2001) 2252–2254.
[28] K. Khanafer, K. Vafai, M. Lightstone, Buoyancy-driven heat transfer enhancement in a two-dimensional enclosure utilizing nanofluids, Int. J. Heat Mass Transf. 46 (2003) 3639–3653.
[29] M. Sheikholeslami, M. Gorji-Bandpy, D.D. Ganji, P. Rana, S. Soleimani, Magnetohydrodynamic free convection of Al2O3-water nanofluid considering thermophoresis and Brownian motion effects, Comput. Fluids 94 (2014) 147–160.
[30] M. Sheikholeslami, M. Gorji-Bandpy, D.D. Ganji, Lattice Boltzmann method for MHD natural convection heat transfer using nanofluid, Powder Technol. 254 (2014) 82–93.
[31] M. Sheikholeslami, M. Gorji-Bandpy, D.D. Ganji, Soheil Soleimani, Heat flux boundary condition for nanofluid filled enclosure in presence of magnetic field, J. Mol. Liq. 193 (2014) 174–184.
[32] Noreen Sher Akbar, Zafar Hayat Khan, S. Nadeem, The combined effects of slip and convective boundary conditions on stagnation-point flow of CNT suspended nanofluid over a stretching sheet, J. Mol. Liq. 196 (2014) 21–25.
[33] Abbas Ibrahim, M.F. El-Amin, A. Salama, Effect of thermal dispersion on free convection in a fluid saturated porous medium, Int. J. for Numerical Methods Heat Fluid Flow 3 (2009) 229–236.
[34] J.H. He, A note on the homotopy perturbation method, Therm. Sci. 14 (2010) 565–568.
[35] J.H. He, Homotopy perturbation method for solving boundary value problems, Phys. Lett. A 350 (2006) 87–88.
[36] M. Rafiq, Y. Malik, T. Abbasi, Solution of nonlinear pull-in behavior in electrostatic micro-actuators by using He's homotopy perturbation method, Comput. Math. Appl. 59 (2010) 2723–2733.
[37] A. Saadatmandi, M. Dehghan, A. Eftekhari, Application of He's homotopy perturbation method for non-linear system of second-order boundary value problems, Nonlinear Anal. Real World Appl. 10 (2009) 1912–1922.
[38] Kh.S. Mekheimer, M.A. El Kot, The micropolar fluid model for blood flow through a tapered artery with a stenosis, Acta Mech. Sinica 24 (2008) 637–644.
[39] V.P. Srivastava, M. Saxena, Suspension model for blood flow through stenotic arteries with a cell-free plasma layer, Math. Biosci. 139 (1997) 79–102.